Accepted Manuscript

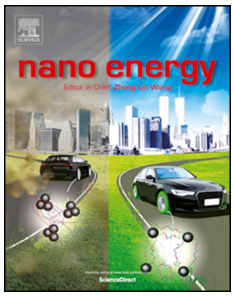

Coloring solar cells with simultaneously high efficiency by low-index dielectric nanoparticles

Yinan Zhang, Shiren Chen, Dejiao Hu, Yi Xu, Sicong Wang, Fei Qin, Yaoyu Cao, Bai-Ou Guan, Andrey Miroshnichenko, Min Gu, Xiangping Li

PII: S2211-2855(19)30471-9

DOI: https://doi.org/10.1016/j.nanoen.2019.05.065

Reference: NANOEN 3779

To appear in: *Nano Energy*

Received Date: 19 February 2019

Revised Date: 17 May 2019

Accepted Date: 24 May 2019

Please cite this article as: Y. Zhang, S. Chen, D. Hu, Y. Xu, S. Wang, F. Qin, Y. Cao, B.-O. Guan, A. Miroshnichenko, M. Gu, X. Li, Coloring solar cells with simultaneously high efficiency by low-index dielectric nanoparticles, *Nano Energy* (2019), doi: https://doi.org/10.1016/j.nanoen.2019.05.065.

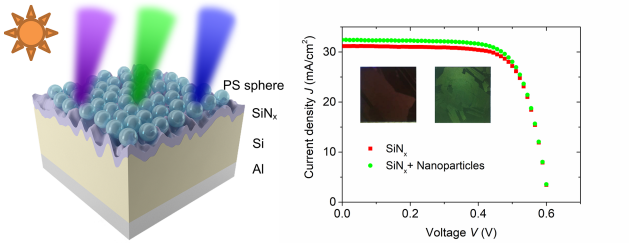

Coloring solar cells with simultaneously high efficiency by low-index dielectric nanoparticles

Yinan Zhang[*1, 2], Shiren Chen[1], Dejiao Hu[1], Yi Xu[3], Sicong Wang[1], Fei Qin[1], Yaoyu Cao[1], Bai-Ou Guan[1], Andrey Miroshnichenko[*4], Min Gu[*2] and Xiangping Li[*1]

[1]*Guangdong Provincial Key Laboratory of Optical Fiber Sensing and Communications, Institute of Photonics Technology, Jinan University, Guangzhou 510632, China*

[2]*Laboratory of Artificial-Intelligence Nanophotonics, School of Science, RMIT University, Melbourne, Victoria 3001, Australia*

[3]*Department of Electronic Engineering, College of Information Science and Technology, Jinan University, Guangzhou 510632, China*

[4]*School of Engineering and Information Technology, University of New South Wales, Canberra, Australian Capital Territory 2600, Australia*

Abstract

Colorful solar cells are highly desired for photovoltaic integration with aesthetically appealing applications such as building facades, self-powered displays and other portable electronic devices. Structural colors by metallic or high-index dielectric nanostructures with judiciously tailored strong resonances are particularly appealing in engineering color appearances of solar cells. However, these prevailing schemes suffering from significant backward scattering power losses for coloration and large intrinsic dissipative losses inevitably degrade solar cell performances, representing a fundamental trade-off between coloring and efficiency improvement. Utilizing a different approach based on all-dielectric low-index submicron-sized spherical nanoparticles, we demonstrate a coloring strategy across the entire visible spectrum with simultaneously improved efficiency. Such nanoparticles exhibit ultra-broadband (300-1200nm) and highly-directional forward scattering features due to the multipolar interferences. Integrating these nanoparticles atop silicon solar cells with an optical impedance matching layer modulates their optical reflection, leading to an extended complementary color palette with noticeable efficiency increase. To the best of our knowledge, this represents the first of its kind that solar cell efficiency can be increased when integrating with nanophotonic structures for coloring. The demonstration of wide coloring and simultaneous light trapping unlocks long-sought strategies to break the color-efficiency trade-off and opens new routes to advanced optoelectronic applications with multi-functionalities.

Key words: dielectric nanoparticles; Mie resonances; structural colors; light

harvesting; solar cells

*Corresponding authors

Email addresses: zhangyinan@jnu.edu.cn; xiangpingli@jnu.edu.cn; min.gu@rmit.edu.au; andrey.miroshnichenko@unsw.edu.au;

Introduction

Solar photovoltaics (PV) offers a major renewable energy source due to their increased energy conversion efficiencies and reduced manufacturing costs in the past few decades.[1,2] One of the major driving forces for PV developments is to integrate with infrastructures such as building façades, walls, fences, awnings, which reduces the cost of the solar power system by eliminating the fixed cost, and with self-powered displays, such as traffic lights, touch screens and other portable and wearable electronic devices. For uptake of this technology by these exciting applications, the aesthetic color appearances of PV cells need to be tailorable with simultaneously high efficiencies.[3-9] Color is an essential aesthetic feature that needs to be considered even beyond the performance for the architectural design and electronic products in daily life. Furthermore, the color pattern design plays a key role in the mobile power application in military camouflage fields. Nevertheless, most of the current solar cells are designed to maximize the solar light absorption and thereby high efficiencies, leading to normally dark and dull colors,[10] which is not visually appealing at all.

Structural color, originating from resonant scattering/absorption or diffraction of photonic nanostructures has emerged as a new route for coloring solar cells. [3-9]

Metallic or high-index dielectric nanostructures showing strong ability in manipulating light-material interaction at visible ranges have attracted great attention for enhancing solar cell performance and photodetector response due to both near-field enhancement and far-field scattering.[11-22] In the meantime, the optical response of such nanostructures is highly dispersive and can produce diverse colors through selective scattering or absorption. [23-34] Plasmonic nanoparticles located on a high-index Si substrate with a dielectric spacing layer can backward scatter the incident light at resonant wavelengths, and thus achieving vivid color displays.[8] The plasmonic nanograting filters were also exploited to produce various colors through the Fabry-Perot cavity resonances and the surface plasmon coupling.[3] However, plasmonic nanostructures unavoidably introduce intrinsic dissipative losses, which are detrimental to solar cell efficiencies. High-index dielectric nanostructures supporting strong geometric Mie resonances with enhanced optical responses, can generate various colors by reflecting light at specific wavelengths through electric and magnetic resonances.[34] For example, Si nanopillar arrays have been imprinted on solar cells to produce green colors. [9] Nevertheless, these high-index Si nanostructures still possess large intrinsic losses, particularly at the UV and visible range. Apart from large dissipative losses, the aforementioned coloring schemes utilizing backward scattering or absorption of light at specific wavelengths deteriorate solar cell efficiencies up to ~10%. This represents a significant power loss of ~9 MWh for a typical 2-kW household system operating for 30 years. Therefore, it remains a fundamental trade-off between color generation and solar efficiencies. Moreover, the

expensive, time-consuming and complexed electron beam lithography and focused ion beam lithography are demanded to pattern these nanostructures with superior device controllability and reliability, restricting them from practical implementation on large-scale solar cells.

Transcending conventional approaches using plasmonic and high-index Si nanostructures based on selective reflection,[3-9] we demonstrate a complementary coloring scheme with simultaneous light trapping by the highly forward scattering from low-index low-loss submicron dielectric nanoparticles prepared through a simple self-assembly transfer method.[35-41] An extended color palette is achieved by the revealed highly forward scattering of low-index nanoparticles which modulates the reflection of SiN_x coated silicon solar cells through multipolar radiative coupling. As a result, comparable and even noticeably improved solar cell efficiencies are observed simultaneously in comparison with the textured solar cells with SiN_x antireflection coating layer. In specific, we achieved environmentally-desired green solar cells by integrating 340 nm polystyrene (PS) nanoparticles atop 43 nm SiN_x layer with an efficiency enhancement of ~4%. The employed low-index PS nanoparticles rely on facile self-assembles empowering a new coloring antireflection scheme in a lithography-free fashion. Together with the scalability and cost-effectiveness of this integration method, our coloring strategy holds great promise for pragmatic colorful and high efficiency solar cells applications in many fields such as building façades and portable self-powered electronic devices.

Results

Low-Index Dielectric Nanoparticle Integrated Solar Cells.

The structure we proposed employs directivity of PS submicron nanoparticles atop the honey-comb textured surface of standard multi-crystalline silicon solar cells with a dielectric spacing layer SiN_x (Figure 1a). The wet-chemically prepared textured surface makes use of the redirection of the light ray because of the geometrical reflection effect at the interface between air and Si, enhancing the light coupling across the entire wavelength band. The SiN_x spacing layer works as an impedance matching layer, serving as reflection modulation and surface passivation as well. These two strategies are widely employed in commercial Si solar cells for enhancing light absorption. Although the SiN_x dielectric layer can be used to control the colors of solar cells through Fabry-Perot resonances, the achieved color palette is quite limited due to the limited degree of freedom (SiN_x thickness). The PS nanoparticles atop the SiN_x layer resonantly interact with the sunlight, facilitating the free-space light coupling due to the highly directional forward scattering based on the mutual interferences between the optical modes within the single nanoparticle. This provides a new degree of freedom for color tunability. At the same time, the optical reflection can be effectively reduced across the entire band and the optical path length of the weakly-absorbed near-infrared light can be enhanced due to the forward scattering induced angular distribution of light entering solar cells. As a result, wide color palette can be achieved with simultaneously improved light absorption, leading to noticeable efficiency increase. Figures 1b and 1c depict a simulated color palette of the integrated device with variant sizes of PS nanoparticles and different thicknesses

of SiN_x spacing layer and their corresponding International Commission on Illumination (CIE) 1931 chromaticity diagram. The bottom row of the color palette and the black circles in CIE diagram represent the colors of the devices with only SiN_x layers and the stars are those integrated with PS nanoparticles atop the SiN_x. Although tuning the thickness of the SiN_x layer can produce colors like yellow and blue, addition of the PS nanoparticle can significantly extend the perceived color palette by simply tuning the nanoparticle size. Figure 1d shows the absorption enhancement of the colorful solar cell under the same configuration of Figure 1b, compared with bare solar cells. It is worth to notice that all the solar cell geometries manifest significant absorption enhancements with the maximum value up to 35%. Even compared with solar cells coated with SiN_x layer of various thicknesses, the absorption still shows noticeable enhancement with tunable colors. Thus, our approach for colorful solar cell offers numerous advantages in terms of color rendering and light trapping as well, providing a highly efficient way for coloring solar cells with high efficiencies. Based on such a library, one can design the solar cell geometry with desired colors and efficiencies at will.

Scattering by a Single PS Nanoparticle

As a starting point, the scattering behaviors of submicron single PS nanoparticle in the air was studied by the finite difference time domain (FDTD) method. Figure 2a illustrates the normalized scattering cross sections of the PS nanoparticle in the air with variant sizes (340 nm, 520 nm and 680 nm). Multiple Mie resonances are excited by the nanoparticle, corresponding to multiple spectral peaks. For the 340 nm sized

nanoparticle, Mie resonances appear at the wavelengths of 320 nm, 400 nm and 550 nm, respectively. These peaks agree well with those observed in the reflection and EQE spectra in the photovoltaic performance measurement. The asymmetric electric field intensity profiles (Figure 2b) in the incident plane for the 340 nm sized nanoparticle at these resonant wavelengths indicate a forward scattering behavior. The far-field scattering patterns shown in Figure 2b also verify this. At these resonant wavelengths (320 nm, 400 nm and 550 nm), light is preferentially forward-scattered while the scattering is relatively symmetric at the off-resonant wavelength like 1100 nm. This is totally distinct from the symmetrical scattering pattern at the resonant wavelengths of plasmonic nanoparticles located in uniform media. It is worth to mention that photonic nanojets with much stronger field localization beneath the spheres can be achieved when the sphere size is about 10 times of the light wavelength.[42] To quantitively study the forward scattering efficiency of the PS nanoparticles, the forward/backward scattering of 340 nm sized PS nanoparticle were extracted from the total scattering, with the results depicted in Figure 2c. Remarkably, the nanoparticle shows an ultra-broadband (300-1200nm) and highly directional scattering with the forward to backward (F/B) scattering ratio up to 30 at the wavelength of 630 nm. By simply tuning the size of the nanoparticle, the maximum ratio can be changed across the entire wavelength range 300-1200nm (Figure S1). It should be mentioned that previous studies of high-index Si nanoparticles reveal rather narrowband forward scattering.[43] Since the forward/backward scattering property stems from the multipolar interference within the nanoparticle, we performed

multipolar decomposition for the purpose of explaining the unique scattering properties of the low-index PS nanoparticles.[44] Figure 2d shows the electric dipole (ED), magnetic dipole (MD), electric quadrupole (EQ) and magnetic octupole (MQ) components were excited in the low-index PS nanoparticle. Clearly, the ED spectrum intersects with the MD at the wavelength of 630 nm, satisfying the first Kerker's condition, resulting in a total suppression of the backward scattering.[43] The ED component in the nanoparticle shows a broadband feature, which can interfere with other optical modes, contributing to the ultra-broadband forward scattering properties.

Once the nanoparticle is placed on the surface of the Si substrate, we observed substantially backward scattering owing to the abrupt refractive index mismatch at the air/Si interface. Particularly, the backward scattering dominates the forward scattering at wavelengths above 550 nm (Figure 3a). This is confirmed by the strong electrical field profile above the nanoparticle as shown in Figure 3c. Introducing the optical impedance matching layer SiN_x can eliminate this strong backward scattering and thus lead to improved absorption in solar cells (Figures 3b and 3d). In the meantime, changing the thickness of the spacing layer can effectively reshape the backward scattering spectra of PS nanoparticles, with the scattering peaks red-shifted and broadened with reduced strengths when the thickness increases (Figure S2). However, the forward scattering spectra show only slight shift while almost preserving the line shape. Since the residual backward scattering determines the complementary color appearances of solar cells, it is expected that vibrant colors with higher saturation can be achieved by introducing an optical impedance matching layer because it can

further narrow the backward scattering spectra of the PS nanoparticle atop the Si substrate.

Color Display of the Integrated PV device

PS nanoparticles were integrated on the surface of standard textured solar cells by a self-assembly transfer method (see Materials and methods for details). The SEM images of the PS nanoparticles on the cell surface are shown in Figures 4a-c. As can be seen, a dense monolayer nanoparticle is formed on the textured surface, with a coverage density of approximately 50%. It should be noted that controlled coverage with highly uniform nanoparticles can be achieved by the improved self-assembly method, exploiting the electrostatic attraction.[45] Unlike those periodic nanoparticles on the flat substrate where the color display is determined by the diffraction effect,[46-48] the textured substrate destroys this regular distribution in the long-range so that the diffraction effect disappears, and the color is only tuned by the residual backward scattering of the PS nanoparticles rather than the diffraction. This is beneficial for the color display because the diffractive colors perceived by the human eyes are angle-dependent while the scattering color remains unchanged in a relatively large viewing angle (Figure S3). The corresponding color images of solar cells are presented in Figure 4d, including solar cells with 340 nm, 520 nm and 680 nm sized nanoparticles (1st column from top to down), 43 nm, 62 nm and 81 nm SiN_x layer (2nd column from top to down) and 340 nm sized nanoparticle atop 43 nm, 62 nm and 81 nm SiN_x layer (3rd column from top to down). Their corresponding CIE chromaticity diagram based on the experimental data is shown in Figure 4e. After coating the PS

nanoparticles on the textured surface with three different sizes (340 nm, 520 nm and 680 nm), the solar cells show purple, green and dark color, respectively. This is due to the directional forward scattering at the multi-order resonant wavelengths, leading to a complementary color display. It should be mentioned that the color saturation is quite low with the coordinates (stars in Figure 4e) mostly located close to the center of the CIE diagram. However, this situation changes significantly once the SiN_x layer is introduced. With the SiN_x layer, the color can be changed with the saturation dramatically increased, as depicted in the color coordinates (triangles) in Figure 4e. The cells exhibit light green, dark green and dark blue, respectively. As a reference, the cells with only the SiN_x layers exhibit light yellow, dark yellow and blue when coated with the SiN_x with a thickness of 43nm, 61nm and 82 nm. This originates from the optical destructive interference in the dielectric films which results in the reflection minima determined by the thickness of the SiN_x layers. The combination of the PS nanoparticles and SiN_x layer significantly extends the color palette with more colors compared with the SiN_x only scheme, as demonstrated in Figure S4.

Figures 4f-h show both the measured (solid) and simulated (dash) reflection spectra of the solar cells integrated with the nanoparticles, the SiN_x dielectric layers, and the combination of these two. The numerical simulation results performed by Lumerical FDTD solver are in a very good agreement with the experiment ones. It is noted that the single nanoparticles show similar resonances to the nanoparticle arrays, with a slight spectrum shifting. The reflection minima of the cells with 340 nm, 520 nm and 680 nm sized nanoparticles occur at 570nm, 620 nm and 750 nm, respectively

while that with 43 nm, 62 nm and 81 nm SiN_x layers are located at 350 nm, 470 nm and 600 nm. Increasing the size of the nanoparticle and the thickness of the SiN_x layer both red-shifts the reflection minima, leading to the color change shown in Figure 4d. With the SiN_x layer inserted between the 340 nm sized PS nanoparticles and the Si substrate, the reflection spectra are narrowed by suppressing the reflection at the short wavelengths. For example, the 43 nm and 62 nm SiN_x layer introduce reflection minima at the wavelength of 420 nm and 450 nm, respectively. This leads to a reflection peak at around 500 nm, corresponding to green colors. This is in coincidence with the backward scattering modulation by the SiN_x layer shown in Figure S2. It should be mentioned that the basic additive colors can be designed following the subtractive color mixing principles. As shown above, the green colors can be created with higher efficiency due to a suppression of the reflection at blue wavelengths by PS nanoparticles and the red region by SiN_x layer. The red and blue colors can follow similar rules with properly designed PS nanoparticle size and SiN_x thickness. Figure S5 gives the detailed reflectance map of the solar cells incorporating nanoparticles and the SiN_x layer, individually and the combination of 340 nm sized nanoparticles with the SiN_x. Distinct dual resonances are introduced by the first-order Mie resonances and the Fabry-Perot resonances, leading to an extension of color palette shown in Figure 1b.

PV Performance of the Integrated Devices

To study the PV performance of the colorful solar cells integrated with PS nanoparticles, external quantum efficiency (EQE), total reflectance and the current

density-voltage (J-V) curves were measured, respectively, with the results shown in Figure 5. Their detailed PV parameters are summarized in Table 1. Figure 5a gives the EQE of the solar cells integrated with the PS nanoparticle of 340 nm, 520 nm and 680 nm, referenced to the bare cells, corresponding to the color appearances shown in the first column of Figure 4d. Clearly, the EQE is improved across the entire band, showing some distinct peaks at the resonant wavelengths of the nanoparticles. This is also verified by the reflection spectra in Figure 5b. The photocurrent calculated from EQE reaches as high as 28.9 mA/cm^2, 29.8 mA/cm^2 and 29.4 mA/cm^2, respectively, corresponding to an enhancement of 4.7%, 8.0% and 6.5%, compared with the 27.6 mA/cm^2 of bare solar cells. The overall performance of the solar cells is also dramatically enhanced with improved photocurrent, as demonstrated in Figure 5c. The efficiencies of the cells can be as high as 11.9%, 12.2% and 11.8%, showing obvious enhancement compared with 11.4% of bare cells.

It is remarkable that addition of the PS nanoparticles atop solar cells with the SiN_x spacing layer can still enhance the efficiency, compared with the case of only SiN_x layer. As an example, Figures 5d-f illustrate the performance of the samples integrated with and without 340 nm sized PS nanoparticles atop 43 nm SiN_x layer, which corresponds green and yellow color, respectively. As shown, the EQE at the wavelength of 600 nm is significantly increased, corresponding to the reflection minimum in Figure 5e. At the short wavelength below 500 nm, the EQE shows slight decrease due to the backward scattering of the nanoparticles. However, the integrated photocurrent from the EQE is increased to 32.3 mA/cm^2 from 31 mA/cm^2,

manifesting an enhancement of 4.2%. The overall efficiency can be as high as 14.2%, with noticeable improvement compared with that (13.7%) of the sample integrated with 43 nm SiN_x. It should be noted that the fill factor (FF) of the cell with SiN_x is larger than without it. This is due to the passivation of the SiN_x, leading to lower surface recombination and thus higher open circuit voltage and the fill factor. It should be mentioned that integrating the PS nanoparticles with variant sizes atop the SiN_x layer with different thicknesses always shows noticeable improvements. This demonstrates the high superiority and flexibility of dielectric nanoparticles in terms of light trapping, compared with the plasmonic nanoparticles possessing large intrinsic absorption losses. When integrating the PS nanoparticles atop 81 nm SiN_X layer, which is the close to the optimal thickness for the solar spectrum, we still observed considerable efficiency enhancement (Figure S6).

Discussion

In conclusion, we have demonstrated a pragmatic coloring strategy for solar cells with simultaneously high-performance light trapping using the low-index submicron dielectric nanoparticles by means of a simple self-assembly method. Both the highly forward scattering features of the low-index dielectric nanoparticles and the optical impedance matching layer play important roles in the color generation. To our knowledge, this represents the first of its kind that solar cell efficiency can be increased simultaneously when integrating with nanophotonic structures for coloring. As a final remark, this method is simple, low cost, scalable and compatible with the commercial solar cell manufacturing processes. Therefore, it can be easily mass

produced by adding one production process of nanoparticle integration. To make this approach long-term feasible and stable in practical applications, one may need additional protection layers and add the photostablizers to prevent the nanoparticles from UV induced degradation.[49] This research provides a novel and pragmatic coloring strategy for integrating photonic nanostructures on PV devices in practical applications.

Materials and Methods

Micro/nanostructure fabrication and characterization

The honey-comb textured surface was created by the HNO_3/HF chemical etching. And the dense monolayer polystyrene sphere was self-assembled on the textured surface of the solar cells according to the following procedures. The commercial PS spheres (2.5% w/v, *Polysciences, Inc.*) were mixed with ethanol in the ratio of 1:1, followed by closely-packed monolayer self-assembly on the surface of the water filled in a peri dish by drop-casting. The alcohol solvent can assist the spreading of the spheres on the water surface so as to form a monolayer assembly. The samples were slightly processed with oxygen plasma to make the surface hydrophilic so that a good contact can be formed during the following transfer and then they were placed at the bottom of the dish before the drop-casting. After the monolayer sphere formation, the water was extracted using a syringe, leaving the samples coated with the sphere in the dish. Then the samples were put in air for natural drying.

Numerical simulations

The simulations, including the reflection spectra, scattering cross-sections of single nanoparticles and field distributions were all calculated by using the finite-difference time-domain (FDTD) method from Lumerical Solutions.[50] And the corresponding optical constants of the materials used in the simulation were obtained from the literature.[51] As for single nanoparticle calculations, a 3-D total field and scattering field source (300-1200 nm) was employed to exclude the scattering light from the incident light. At the same time, six transmission monitors were positioned outside the light source box to collect the scattered light. The boundary conditions were set as perfectly matched layers (PMLs) to eliminate the reflected light from the boundaries. To acquire the electric field profiles, a two-dimensional field monitor was positioned through the center of the nanoparticles. For the reflection spectra calculation, a plane wave source with the same wavelength range was employed to illuminate a Si wafer with uniformly and randomly distributed nanoparticles on the surface. And a transmission monitor placed above the light source was used to obtain the reflection of the solar cells. As a comment, due to the spherically symmetric feature of the nanoparticles and the point contact between the nanoparticles and the solar cells, our model based on a flat Si wafer is valid for the real scenario with textured surface and there is trivial effect on the forward/backward scattering properties (Fig. 4), although the near field pattern and position might be noticeably influenced as illustrated in Ref. 52.

Solar cell fabrication and characterization

The experimentally used textured Si solar cells were fabricated on p-type

multi-crystalline Si wafers with a thickness of ~200 μm. Firstly, we removed the saw damage surface layers using wet chemical etching and the wafers were then transferred to the standard RCA cleaning bath. After this, the PN junction of the cells were created by a high temperature (~850 ℃) diffusion process using $POCl_3$ as the dopant source. To remove the accompanying phospholipase glass formed in this process, we then put the wafers in 5% HF solution for ~10 mins. The optical index matching layer SiN_x with various thicknesses were deposited through the plasmon enhanced chemical vapor deposition system (Oxford Instruments, PLASMALAB 100 PECVD) by controlling the deposition time. The front metal grid electrodes were fabricated by the photolithography procedure while the back electrodes were produced by depositing a thick layer of Al (~1 μm) followed by annealing to form the ohmic contact. The current-voltage curves were measured by a commercial system (Newport Oriel I-V station), equipped with a class AAA solar simulator and a source meter (Keithley 2400) at the temperature of 25 ℃. The external quantum efficiency data were acquired by PV Measurements X10 in the wavelength range 300-1200 nm with 5 nm interval. While the reflectance of the solar cells was measured by the UV–VIS-NIR spectrophotometer (Perkin Elmer, Lambda 1050) with an integrating sphere to collect the diffused reflection by the micro/nano structures.

Acknowledgments

This work was supported by National Key R&D Program of China (YS2018YFB110012), National Natural Science Foundation of China (Grant Nos. 61605065, 61522504), Guangdong Provincial Innovation and Entrepreneurship Project (Grant Nos. 2016ZT06D081) and Guangzhou

Science and Technology Program (Grant No. 201804010322). A.E.M acknowledges the support from the Australian Research Council and UNSW Scientia Fellowship.

References

1. Polman, A.; Knight, M.; Garnett, E. C.; Ehrler, B.; Sinke, W. C. Photovoltaic materials: Present efficiencies and future challenges. *Science* **2016,** 352, aad4424.

2. Green, M. A.; Hishikawa, Y.; Warta, W.; Dunlop, E. D.; Levi, D. H.; Hohl-Ebinger, J.; Ho-Baillie, A. W. H. Solar cell efficiency tables (version 51). *Prog. Photovoltaics Res. Appl.* **2017**, 25, 668-676.

3. Park, H. J.; Xu, T.; Lee, J. Y.; Ledbetter, A.; Guo, L. J. Photonic color filters integrated with organic solar cells for energy harvesting. *ACS Nano* **2011**, 5, 7055-7060.

4. McFarlane, T. D.; De Castro, C. S.; Holliman P. J.; Davies, M. L. Improving the light harvesting and colour range of methyl ammonium lead tri-bromide (MAPbBr3) perovskite solar cells through co-sensitisation with organic dyes. *Chem. Commun.*, **2019**, 55, 35-38.

5. Zhang, W.; Anaya, M.; Lozano, G.; Calvo, M. E.; Johnston, M. B.; Míguez, H.; Snaith, H. J. Highly Efficient Perovskite Solar Cells with Tunable Structural Color. *Nano Lett*. **2015**, 15, 1698-1702.

6. Chen, F.; Wang, S.-W.; Liu, X.; Ji, R.; Li, Z.; Chen, X.; Chen, Y.; Lu, W. Colorful solar selective absorber integrated with different colored units. *Opt. Express* **2016**, 24, A92-A103.

7. Jiang, Y.; Luo, B.; Jiang, F.; Jiang, F.; Fuentes-Hernandez, C.; Liu, T.; Mao, L.; Xiong, S.; Li, Z.; Wang, T.; Kippelen, B.; Zhou, Y. Efficient Colorful Perovskite Solar Cells Using a Top Polymer Electrode Simultaneously as Spectrally Selective Antireflection Coating. *Nano Lett.* **2016**, 16, 7829-7835.

8. Wen, L.; Chen, Q.; Hu, X.; Wang, H.; Jin, L.; Su, Q. Multifunctional Silicon Optoelectronics Integrated with Plasmonic Scattering Color. *ACS Nano* **2016**, 10, 11076-11086.

9. Neder, V.; Luxembourg, S. L.; Polman, A. Efficient colored silicon solar modules using integrated resonant dielectric nanoscatterers. *Appl. Phys. Lett.* **2017,** 111, 073902.

10. Yang, J.; Luo, F.; Kao, T.; Li, X.; Ho, G.; Teng, J.; Luo, X.; Hong, M. Design and fabrication of broadband ultralow reflectivity black Si surfaces by laser micro/nanoprocessing. *Light Sci. Appl.* **2014**, 3, e185

11. Atwater, H. A.; Polman, A. Plasmonics for improved photovoltaic devices. *Nat. Mater.* **2010**, 9, 205-213.

12. Brongersma, M. L.; Cui, Y.; Fan, S. Light management for photovoltaics using high-index nanostructures. *Nat. Mater.* **2014,** 13, 451-460.

13. Zhang, Y.; Stokes, N.; Jia, B.; Fan, S.; Gu, M. Towards ultra-thin plasmonic silicon wafer solar cells with minimized efficiency loss. *Sci. Rep.* **2014**, 4, 4939.

14. Zhang, Y.; Jia, B.; Gu, M. Biomimetic and plasmonic hybrid light trapping for highly efficient ultrathin crystalline silicon solar cells. *Opt. Express* **2016**, 24, A506-A514.

15. Zhao, F.; Arnob, M. M. P.; Zenasni, O.; Lia J.; Shih W.-C. Far-field plasmonic coupling in 2-dimensional polycrystalline plasmonic arrays enables wide tunability with low-cost nanofabrication *Nanoscale Horiz.*, **2017**,2, 267.

16. Wang, K. X.; Yu, Z.; Liu, V.; Cui, Y.; Fan, S. Absorption Enhancement in Ultrathin Crystalline Silicon Solar Cells with Antireflection and Light-Trapping Nanocone Gratings. *Nano Lett.* **2012,** 12, 1616-1619.

17. Zhang, Y.; Ouyang, Z.; Stokes, N.; Jia, B.; Shi, Z.; Gu, M. Low cost and high performance Al nanoparticles for broadband light trapping in Si wafer solar cells. *Appl. Phys. Lett.* **2012**, 100, 151101-4.

18. Lee, D. H.; Kwon, J. Y.; Maldonado, S.; Tuteja, A.; Boukai, A. Extreme light absorption by multiple plasmonic layers on upgraded metallurgical grade silicon solar cells. *Nano Lett.* **2014**, 14, 1961-1967.

19. Li, G.; Li, H.; Ho, J. Y. L.; Wong, M.; Kwok, H. S. Nanopyramid Structure for Ultrathin c-Si Tandem Solar Cells. *Nano Lett.* **2014**, 14, 2563-2568.

20. Huang, Y.; Yan, J.; Ma C.; Yang, G. Active tuning of the Fano resonance from a Si nanosphere dimer by the substrate effect. *Nanoscale Horiz.*, **2019**, 4, 148

21. Zhang, Y.; Xu, Y.; Chen, S.; Lu, H.; Chen, K.; Cao, Y.; Miroshnichenko, A.; Gu, M.; Li, X. Ultra-Broadband Directional Scattering by Colloidally Lithographed High-Index Mie Resonant Oligomers and Their Energy-Harvesting Applications. *ACS Appl. Mater. Interfaces.* **2018**, 10, 16776-16782.

22. Tong, J.; Suo, F.; Ma, J.; Tobing, L. Y. M.; Qian, L.; Zhang, D. Surface plasmon enhanced infrared photodetection. *Opto-Electronic Advances*, **2019**, 2, 180026.

23. Gu, Y.; Zhang, L.; Yang, J. K. W.; Yeo, S. P.; Qiu, C.-W. Color generation via subwavelength plasmonic nanostructures. *Nanoscale* **2015,** 7, 6409-6419.

24. Zhang, X.; Li, P.; Barreda, A.; Gutie'rrez, Y.; Gonza'lez, F.; Moreno, F.; Everitt H. O.; Liu J. Size-tunable rhodium nanostructures for wavelength-tunable ultraviolet plasmonics. *Nanoscale Horiz.*, **2016**, 1, 75.

25. Zhang, Y.; Shi, L.; Hu, D.; Xie, S.; Lu, Y.; Cao, Y.; Zhu, Z.; Jin, L.; Guan, B.; Rogge, S.; Li, X. Full-Visible Multifunctional Aluminium Metasurfaces by In Situ Anisotropic Thermoplasmonic Laser Printing. *Nanoscale Horiz.*, **2019**, 4, 601-609.

26. Duan, X.; Kamin, S.; Liu, N. Dynamic plasmonic colour display. *Nat. Commun.* **2017**, 8, 14606.

27. Duan, X.; Liu, N. Scanning Plasmonic Color Display. *ACS Nano.* **2018**, 12 (8), 8817–8823

28. Sun, S.; Zhou, Z.; Zhang, C.; Gao, Y.; Duan, Z.; Xiao, S.; Song, Q. All-Dielectric Full-Color Printing with TiO_2 Metasurfaces. *ACS Nano* **2017,** 11, 4445-4452.

29. Proust, J.; Bedu, F.; Gallas, B.; Ozerov, I.; Bonod, N. All-Dielectric Colored Metasurfaces with Silicon Mie Resonators. *ACS Nano* **2016,** 10, 7761-7767.

30. Wang, H.; Wang, X.; Yan, C.; Zhao, H.; Zhang, J.; Santschi, C.; Martin, O. J. F. Full Color Generation Using Silver Tandem Nanodisks. *ACS Nano* **2017,** 11, 4419-4427.

31. Goh, X. M.; Zheng, Y.; Tan, S. J.; Zhang, L.; Kumar, K.; Qiu, C.-W.; Yang, J. K. W. Three-dimensional plasmonic stereoscopic prints in full colour. *Nat. Commun.* **2014,** 5, 5361.

32. Hu, D.; Lu, Y.; Cao, Y.; Zhang, Y.; Xu, Y.; Li, W.; Gao, F.; Cai, B.; Guan, B.; Qiu, C.; Li, X. Laser-Splashed Three-Dimensional Plasmonic Nanovolcanoes for Steganography in Angular Anisotropy. *ACS Nano* **2018,** 12, 9233-9239.

33. Olson, J.; Manjavacas, A.; Basu, T.; Huang, D.; Schlather, A. E.; Zheng, B.; Halas, N. J.; Nordlander, P.; Link, S. High Chromaticity Aluminum Plasmonic Pixels for Active Liquid Crystal Displays. *ACS Nano* **2016**, 10, 1108-1117.

34. Kuznetsov, A. I.; Miroshnichenko, A. E.; Brongersma, M. L.; Kivshar, Y. S.; Luk'yanchuk, B. Optically resonant dielectric nanostructures. *Science* **2016,** 354, aag2472

35. Chen, L.; Zhou, Y.; Wu, M.; Hong, M. Remote-mode microsphere nano-imaging: new boundaries for optical microscopes. *Opto-Electronic Advances* **2018**, 1, 170001

36. Wang, Z.; Guo, W.; Li, L.; Luk'yanchuk, B.; Khan, A.; Liu, Z.; Chen, Z.; Hong, M. *Nat. Commun.* **2011**, 2, 218.

37. Luk'yanchuk, B.; Paniagua-Domínguez, R.; Minin, I.; Minin, O. and Wang, Z. Refractive index less than two: photonic nanojets yesterday, today and tomorrow. *Opt. Mater. Express* **2017**, 7, 1820-1847.

38. Grandidier, J.; Callahan, D. M.; Munday, J. N.; Atwater, H. A. Light Absorption Enhancement in Thin-Fil8m Solar Cells Using Whispering Gallery Modes in Dielectric Nanospheres. *Adv. Mater*. **2011**, 23, 1272-1276.

39. Kang, G.; Park, H.; Shin, D.; Baek, S.; Choi, M.; Yu, D.-H.; Kim, K.; Padilla, W. J. Broadband Light-Trapping Enhancement in an Ultrathin Film a-Si Absorber Using Whispering Gallery Modes and Guided Wave Modes with Dielectric Surface-Textured Structures. *Adv. Mater.* **2013,** 25, 2617-2623.35.

40. Wang, B.; Leu, P. W. High index of refraction nanosphere coatings for light trapping in crystalline silicon thin film solar cells. *Nano Energy* **2015,** 13, 226-232.

41. Wang, B.; Gao, T.; Leu, P. W. Broadband light absorption enhancement in ultrathin film crystalline silicon solar cells with high index of refraction nanosphere arrays. *Nano Energy* **2016,** 19, 471-475.

42. Wang, Z.; Luk'yanchuk, B.; Hong, M.; Lin, Y. and Chong, T. C. Energy flow around a small particle investigated by classical Mie theory, *Phys. Rev. B* **2004**, 70, 035418

43. Fu, Y.; Kuznetsov, A; Miroshnichenko, A; Yu Y; Luk'yanchuk, B. Directional visible light scattering by silicon nanoparticles. *Nat. Commun.* **2013**, 4, 1527.

44. Grahn, P.; Shevchenko, A.; Kaivola, M. Electromagnetic multipole theory for optical nanomaterials. *New J. Phys.* **2012**, 14, 093033.

45. Reineck, P.; Lee, G. P.; Brick, D.; Karg, M.; Mulvaney, P.; Bach U. A Solid-State Plasmonic Solar Cell via Metal Nanoparticle Self-Assembly. *Adv.Mater.* **2012**, 24, 4750–4755

46. Moon, G. D.; Lee, T. I.; Kim, B.; Chae, G.; Kim, J.; Kim, S.; Myoung, J.-M.; Jeong, U. Assembled monolayers of hydrophilic particles on water surfaces. *ACS Nano* **2011,** 5, (11), 8600-8612.

47. Vogel, N.; de Viguerie, L.; Jonas, U.; Weiss, C. K.; Landfester, K. Wafer-Scale Fabrication of Ordered Binary Colloidal Monolayers with Adjustable Stoichiometries. *Adv. Funct. Mate.* **2011,** 21, 3064-3073.

48. Zheng, P.; Kasani S.; Wu N. Converting plasmonic light scattering to confined light absorption and creating plexcitons by coupling a gold nano-pyramid array onto a silica–gold film. *Nanoscale Horiz.* **2019**, 4, 516-525.

49. Ali, G.; El-Hiti, G. A.; Tomi, I. H. R.; Haddad, R.; Al-Qaisi, A. J.; Yousif E. Photostability and Performance of Polystyrene Films Containing 1,2,4-Triazole-3-thiol Ring System Schiff Bases. *Molecules* **2016**, 21(12), 1699

50. FDTD solutions (www.lumerical.com)

51. Palik, E. D. Handbook of Optical Constants of Solids; Academic:New York, 1985.

52. Wang, Z. B.; Hong, M. H. Angle effect in laser nanopatterning with particle-mask, *J. Appl. Phys.* **2004**, 96, 6845.

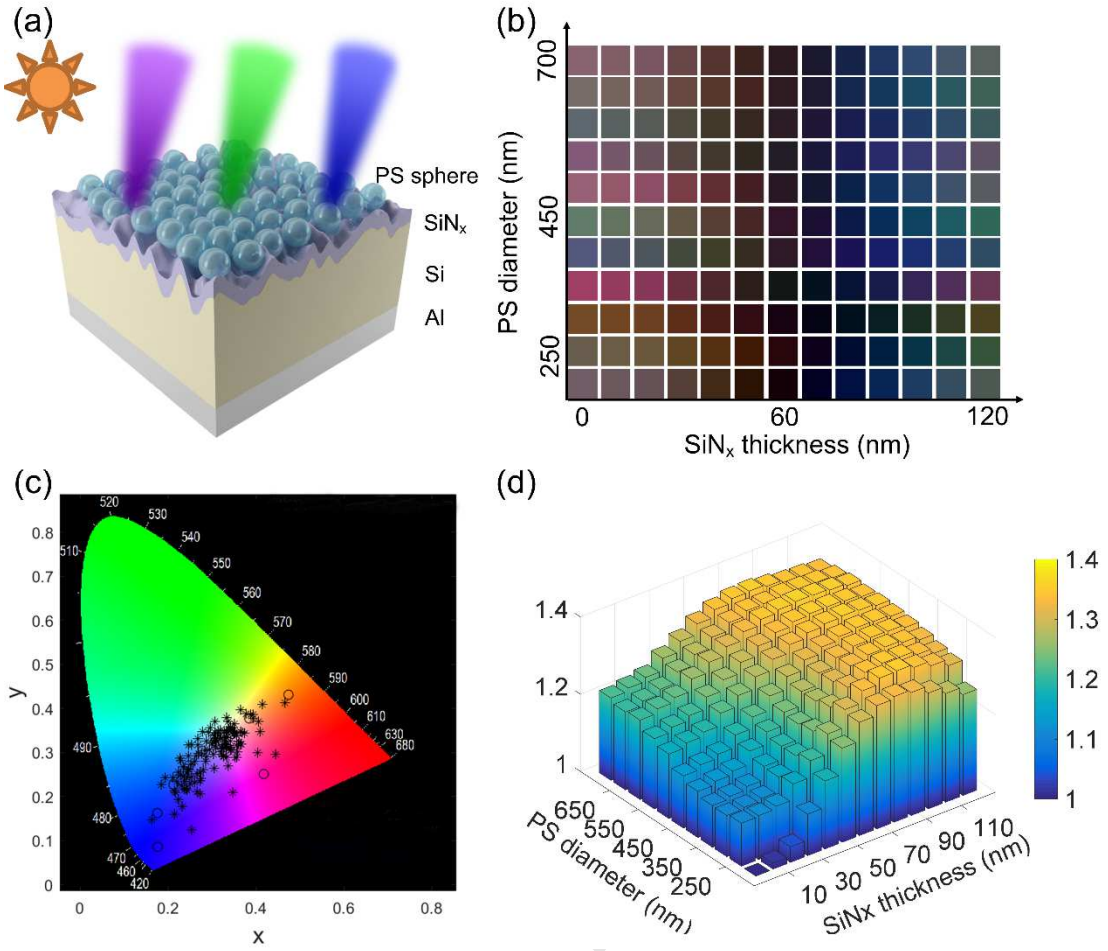

Figure 1. (a) Schematic diagram of the colorful solar cell integrated with the low-index dielectric nanoparticles. (b) The color palette of the solar cells integrated with varied size of PS nanoparticles and thickness of SiN_x spacing layer. The bottom row palette represents the solar cells with SiN_x individually. (c)The corresponding International Commission on Illumination (CIE) 1931 chromaticity diagram based on the simulated reflectance. (circles: SiN_x, stars: nanoparticle + SiN_x). (d) The absorption enhancement of the colorful solar cells under the same configuration, referenced to bare solar cells.

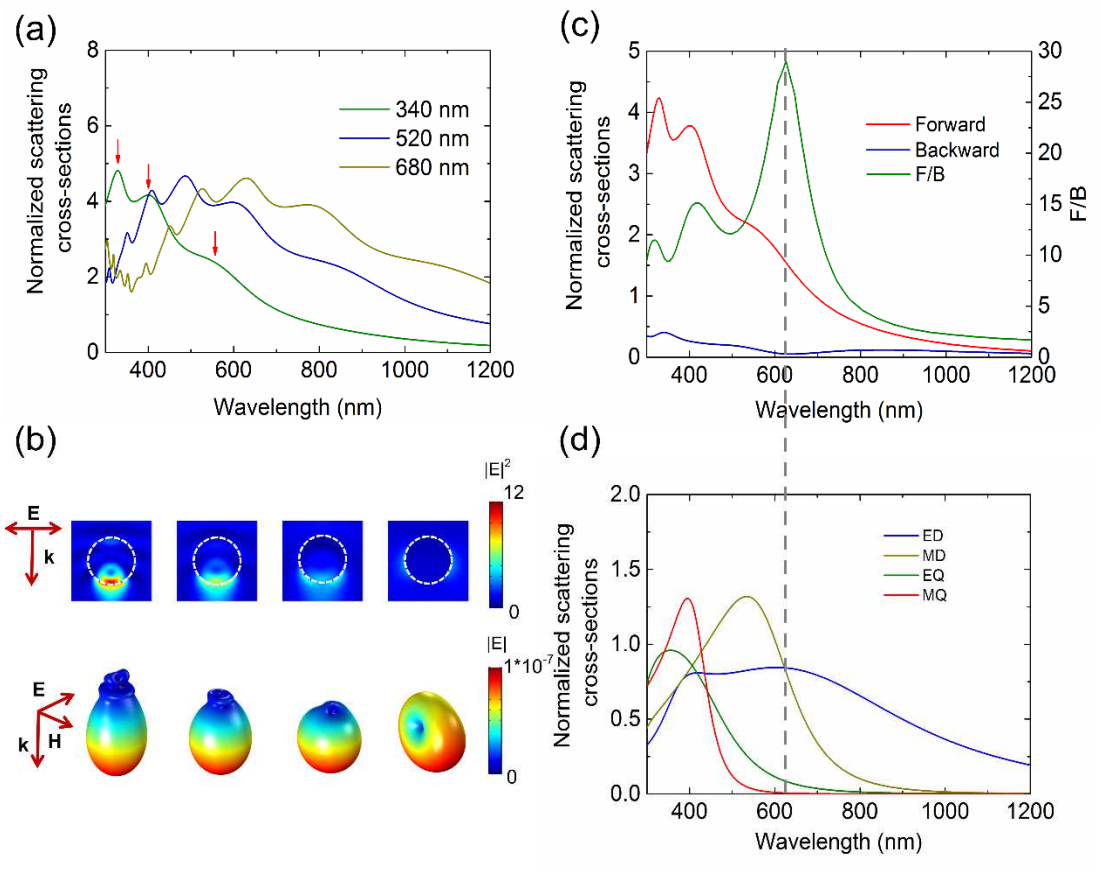

Figure 2. Mie resonance analysis of the single low-index polystyrene (PS) nanoparticle in the air. (a) Scattering cross-sections of the PS nanoparticles with diameters of 340nm, 520nm and 680nm in the air. (b) Electrical near-field intensity profiles and far-field scattering patterns of the 340 nm nanoparticle at the three resonance wavelengths 320 nm, 400 nm and 550 nm and the wavelength 1100 nm, off the resonance. (c) Forward and backward scattering cross-sections of the 340 nm nanoparticles and their ratio F/B. (d) The electric dipole (ED), magnetic dipole (MD), electric quadrupole (EQ) and magnetic quadrupole (MQ) components of the scattering cross-section for 340 nm nanoparticles.

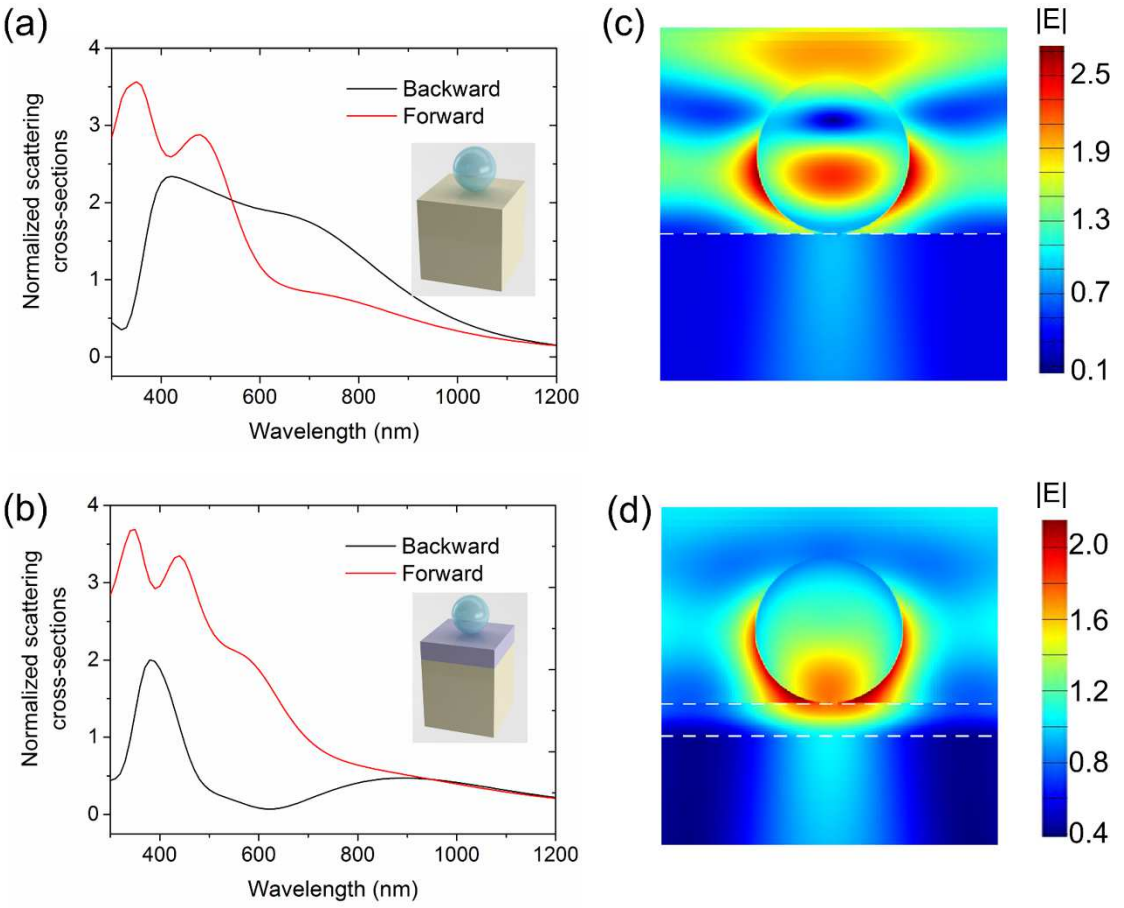

Figure 3. Substrate effect on the scattering of the single polystyrene (PS) nanoparticle. (a, b) Forward and backward scattering cross-sections of the 340 nm PS nanoparticle located on the surface of an infinite Si substrate and on the Si with 80 nm SiN_x spacing layer. (c, d) The electrical field intensity profiles at the wavelength of 600 nm for the two cases.

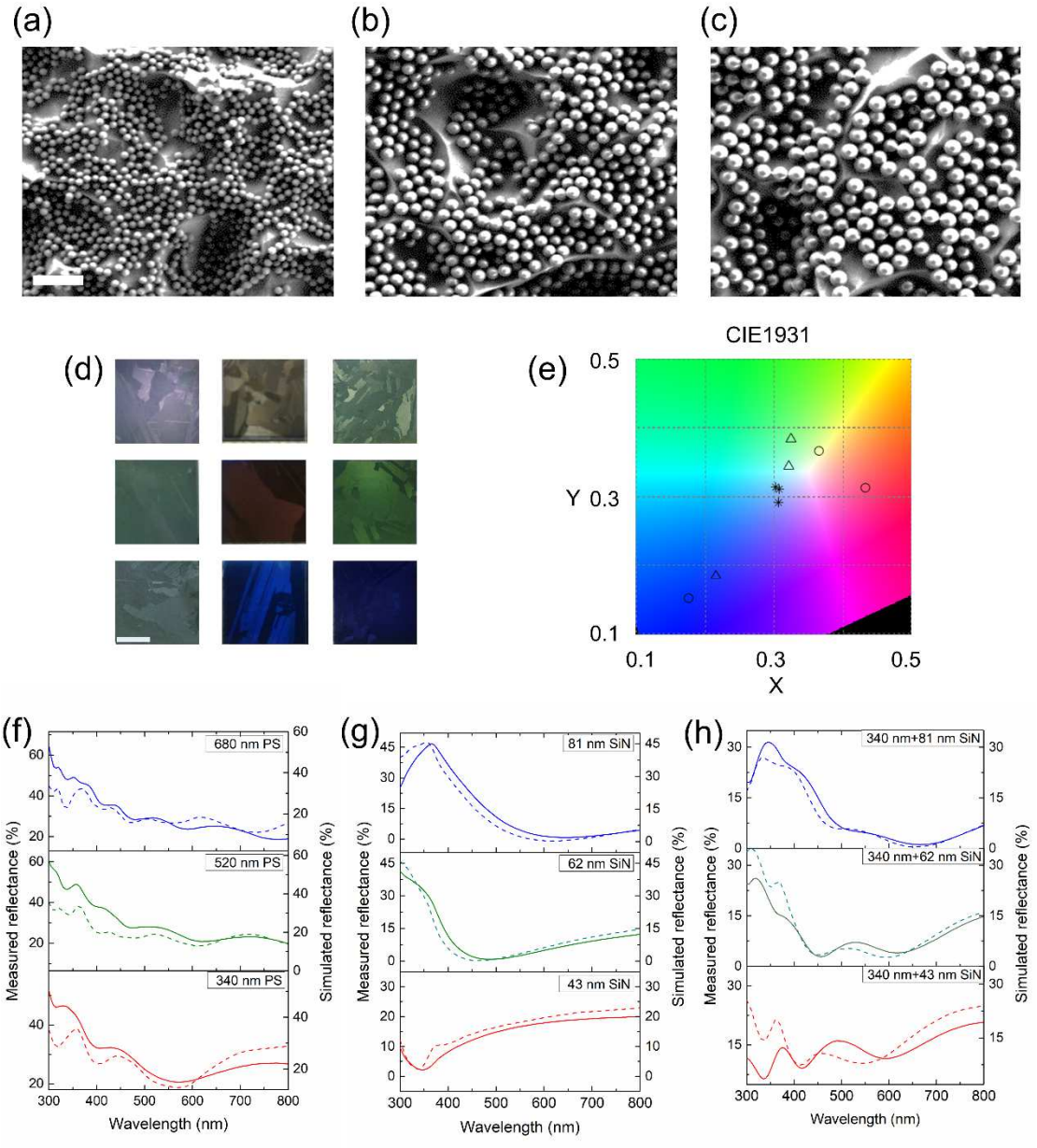

Figure 4. SEM images of the surfaces of honey-comb textured solar cells integrated with PS nanoparticles with a diameter of (a) 340 nm (b) 520 nm (c) 680 nm. The images use the same scale bar. (Scale bar: 2 μm).(d) Photos of the colorful solar cells (2.5×2.5 cm) integrated with the 340 nm, 520 nm and 680 nm nanoparticles (1st column from top to down), 43 nm, 62 nm and 81 nm SiN_x layer (2nd column from top to down) and 340 nm nanoparticle atop 43 nm, 62 nm and 81 nm SiN_x layer (3rd column from top to down). (Scale bar: 1 cm) (e) The corresponding International Commission on Illumination (CIE) 1931 chromaticity diagram based on the

experimental data. (star: nanoparticle, circle: SiN_x, triangle: nanoparticle + SiN_x). The measured (solid lines) and simulated (dashed lines) reflectance of the solar cells integrated with (f) 340 nm, 520 nm and 680 nm nanoparticles, (g) 43 nm, 62 nm and 81 nm SiN_x and (h) 340 nm nanoparticles atop 43 nm, 62nm and 81 nm SiN_x layer.

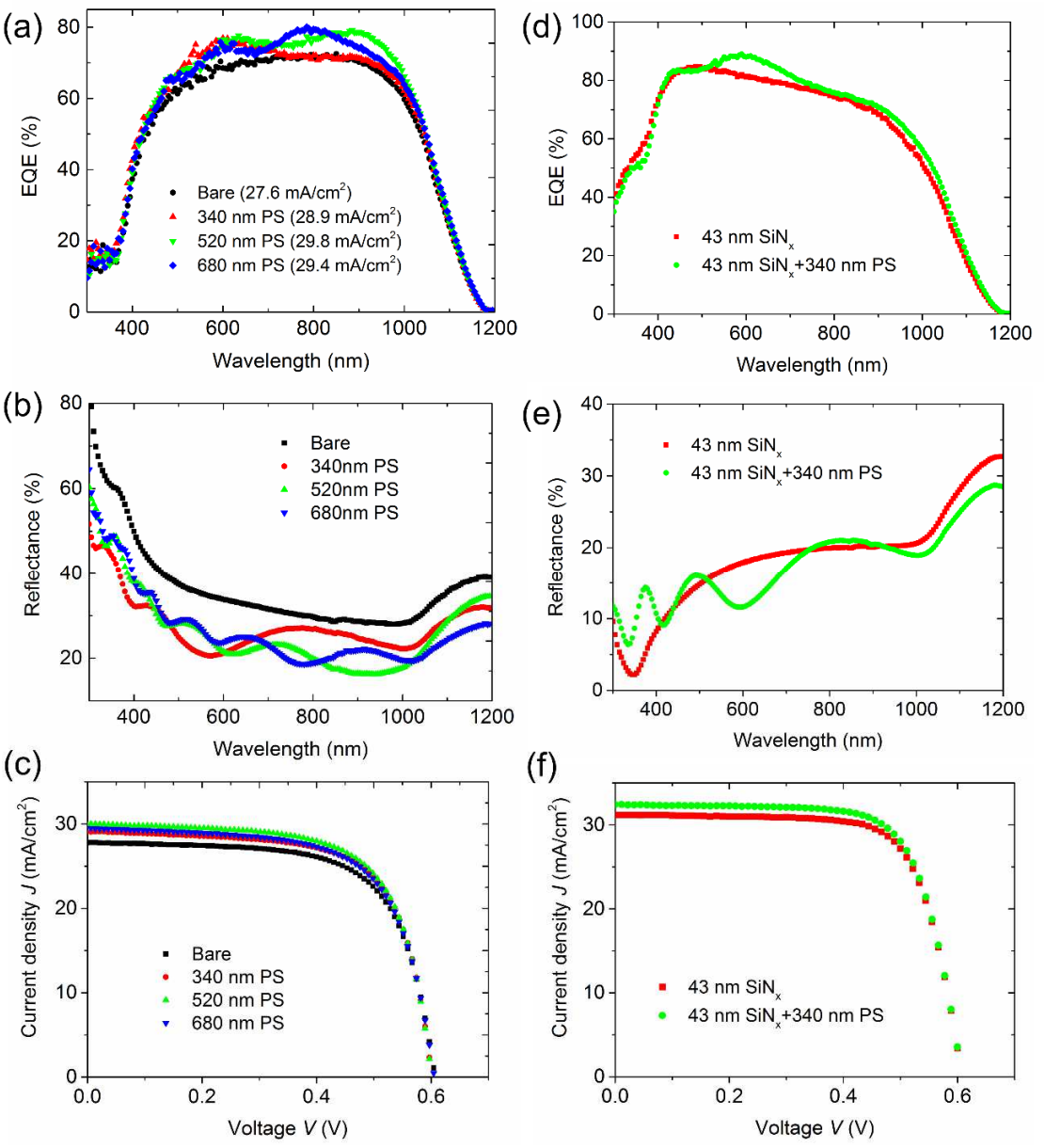

Figure 5. Photovoltaic performance of the solar cells. (a-c) External quantum efficiency (EQE)、total reflectance and current density-voltage (J-V) curves of the solar cells with only PS

nanoparticles on the surface, referenced to the bare case. (d-f) EQE, reflectance and J-V curves of the solar cells with 43 nm SiN_x layer and 340 nm nanoparticles atop the SiN_x layer.

Table 1. The electrical parameters of the solar cells

Solar cell geometry	V_{oc} (V)	J_{sc}(mA/cm²)	FF(%)	E_{ff}(%)	CIE 1931 (x, y)
Bare	0.606	27.8	67.4	11.4	
340 nm PS nanoparticle	0.600	29.1	68.3	11.9	0.30, 0.29
520 nm PS nanoparticle	0.599	30	67.6	12.2	0.30, 0.31
680 nm PS nanoparticle	0.604	29.5	66.4	11.8	0.31, 0.31
43 nm SiN_x	0.607	31.2	72.2	13.7	0.37, 0.37
62 nm SiN_x	0.604	32.8	74.1	14.7	0.43, 0.31
81 nm SiN_x	0.609	34.3	73.8	15.3	0.18, 0.15
340 nm PS + 43 nm SiN_x	0.608	32.4	71.8	14.2	0.32, 0.34
340 nm PS + 62 nm SiN_x	0.604	32.6	74.5	14.7	0.33, 0.38
340 nm PS + 81 nm SiN_x	0.609	34.8	73.2	15.5	0.21, 0.18

Yinan Zhang is an associate professor at Institute of Photonics Technology, Jinan University, Guangzhou, China. He received his PhD degree from Centre for Micro-Photonics at Swinburne University of Technology in 2014. His research interests are solar energy harvesting and laser nanomaterial interactions. He was awarded the prestigious 2014 Chinese Government Scholarship for Outstanding Self-financed Students Abroad.

Shiren Chen is currently a master student at Institute of Photonics Technology, Jinan University, Guangzhou, China. He obtained his bachelor's degree from University of Jinan, Shandong, China. His current research focuses on laser fabrication and nanoplasmonics.

Dejiao Hu received his PhD degree from Sichuan University in 2016. Now he is a postdoctoral researcher in the nanophotonic devices group in the Institute of Photonics Technology, Jinan University, Guangzhou, China. His research is mainly focused on nanoplasmonics and metasurfaces.

Yi Xu received his bachelor degree and PhD degree both from South China Normal University. He visited Nonlinear Physics Center of Australian National University during 2010-2011 as a joint PhD student. His research is focused on manipulation of light-matter interaction utilizing structured matter and light. Dr. Xu has published over 40 peer-review papers, including Nat. Communications, Phys. Rev. Lett., Phys. Rev. A/B (R) and Laser Photon. Review. He received Wang Da-Heng Optical Awards from Chinese Optical Society. He also serves as a

topical Editor of Acta Optica Sinica.

Sicong Wang received his PhD degree from Sun Yat-Sen University in 2015. Now he is a lecturer in the Institute of Photonics Technology, Jinan University. His research is mainly focused on manipulations of vector beams, all-optical magnetic recording, and superresolution.

Fei Qin is currently an associate professor at Institute of Photonics Technology, Jinan University, Guangzhou, China. He Received his PhD degree in Optics from Institute of Physics, Chinese Academy of Sciences. His research interest focuses on nanophotonics, planar metalens, metasurfaces, and their applications in light manipulation and label-free super-resolution imaging.

Yaoyu Cao is a professor in Institute of Photonics Technology, at Jinan University, where he has been since 2016. He received a B. S. from University of Science and Technology of China in 2004. He completed his PhD at Technical Institute of Physics and Chemistry, Chinese Academy of Sciences in 2009. From 2009 to 2016, he worked at Centre for Micro-Photonics in Swinburne University in Australia. His research interests span over direct laser writing, functional optical nanomaterials and optical super-resolution technique.

Bai-Ou Guan received the Ph.D. degrees in optics from Nankai University, Tianjin, China, in 2000. From 2000 to 2005, he was with The Hong Kong Polytechnic University, first as a Research Associate, and then as a Postdoctoral Research Fellow. From 2005 to 2009, he was with Dalian University of Technology, Dalian, as a Full Professor. In 2009, he joined Jinan University, Guangzhou, where he founded the Institute of Photonics Technology. His current research interests include fiber optic devices and technologies, optical fiber sensors, biomedical photonic sensing and imaging, and microwave photonics.

Andrey Miroshnichenko obtained his PhD in 2003 from the Max-Planck Institute for Physics of Complex Systems in

Dresden, Germany. In 2004 he joined the Nonlinear Physics Centre at ANU. During that time, he made fundamentally significant contributions to the field of photonic crystals and bringing the concept of the Fano resonances to nanophotonics. In 2017 he has moved to the University of New South Wales Canberra and got very prestigious UNSW Scientia Fellowship. The topics of his research are nonlinear nanophotonics, nonlinear optics, resonant interaction of light with nanoclusters, including optical nanoantennas and metamaterials.

Min Gu is Executive Chancellor and Distinguished Processor of University of Shanghai for Science and Technology. He was Distinguished Professor and Associate Deputy Vice-Chancellor at RMIT University and a Laureate Fellow of the Australian Research Council. He is an elected Fellow of the Australian Academy of Science and the Australian Academy of Technological Sciences and Engineering as well as Foreign Fellow of the Chinese Academy of Engineering. He is also an elected fellow of the AIP, the OSA, the SPIE, the InstP, and the IEEE. Professor Gu is a winner of the 2019 Dennis Gabor Award of SPIE.

Xiangping Li received his PhD degree from Swinburne University of Technology in 2009. Now he is a professor and research leader of nanophotonic devices group in the Institute of Photonics Technology, Jinan University. His research is mainly focused on nanophotonics, nanoplasmonics and metasurfaces.

Highlights

- Ultra-broadband and highly forward scattering from low-index dielectric nanoparticles
- Mie resonances as well as Fabry-Perot resonances are employed to tune the color appearances of solar cells
- Wide coloring with simultaneously higher efficiency is achieved